Available online at www.sciencedirect.com

ScienceDirect

Geochimica et Cosmochimica Acta 185 (2016) 198–215

Geochimica et Cosmochimica Acta

www.elsevier.com/locate/gca

Petrogenesis of high-CaO lavas from Mauna Kea, Hawaii: Constraints from trace element abundances

Shichun Huang [a,*], Munir Humayun [b]

[a] Department of Geoscience, University of Nevada, Las Vegas, NV 89154, United States

[b] National High Magnetic Field Laboratory and Department of Earth, Ocean, & Atmospheric Science, Florida State University, Tallahassee, FL 32310, United States

Received 23 July 2015; accepted in revised form 30 March 2016; available online 6 April 2016

Abstract

The role of a mafic component in the petrogenesis of Oceanic Island Basalts (OIBs) is highly debated. As the best studied OIB, Hawaiian lavas provide critical insights into OIB genesis. At a given MgO content, the CaO content in the melt has been used to distinguish between partial melts of peridotite and garnet pyroxenite/eclogite. However, calculations using the BATCH program show that CaO contents in volatile-free melts saturated with all four phases, garnet, clinopyroxene, orthopyroxene and olivine, are controlled by both degrees of partial melting and source compositions, and low melt CaO content is not diagnostic of partial melts from garnet pyroxenite/eclogite. This is an important consideration in understanding the origin of high-CaO lavas recovered from the Hawaii Scientific Drilling Project (HSDP). Detailed geochemical and isotopic studies have been focused on the HSDP high- and low-SiO_2 group lavas, and high-CaO lavas were not well studied because they were not included in the original reference suite samples. Here, we report trace element abundances obtained on a suite of high-CaO glasses and compared the trace element abundances of high-CaO lavas to those in high- and low-SiO_2 lavas. When normalized to the average composition of low-SiO_2 lavas, high-CaO lavas form a U-shaped trace element pattern, enriched in both the most incompatible (Nb, Th) and the least incompatible (Sc, V) elements. This compositional distinction is best explained if high-CaO parental magma represents a mixture of a low degree partial melt of the low-SiO_2 mantle source with a high degree (>80%) partial melt derived from a mafic cumulate component. This mafic cumulate must be clinopyroxene-rich, and it could be delaminated mafic cumulate formed under arcs during continent formation, lower continental crust, recycled lower oceanic crust, or high pressure cumulates from a magma chamber.

Keywords: Hawaii; Mantle plume; Mafic cumulates; Trace elements; Mantle heterogeneity

1. INTRODUCTION

Subduction of oceanic crust into the Earth's mantle and delamination of lower oceanic and continental crust introduce mafic components (e.g., Hofmann and White, 1982; McKenzie and O'Nions, 1983; Lee et al., 2012; Jagoutz and Schmidt, 2013). However, the role of a mafic lithology, pyroxenite or eclogite, in generating Ocean Island Basalts (OIBs) is hotly debated (e.g., Hauri, 1996; Lassiter and Hauri, 1998; Wagner and Grove, 1998; Chauvel and Hémond, 2000; Huang and Frey, 2005; Huang et al., 2005; Sobolev et al., 2005, 2007; Herzberg, 2006; Kogiso and Hirschmann, 2006; Salters et al., 2006; Jackson and Dasgupta, 2008; Dasgupta et al., 2010; Putirka et al., 2011; Jackson et al., 2012; Rhodes et al., 2012; Pietruszka et al., 2013; Herzberg et al., 2014; Frey et al., this issue). On both global and local scales, major element contents and radiogenic isotope ratios in OIBs are correlated,

* Corresponding author.
E-mail address: shichun.huang@unlv.edu (S. Huang).

http://dx.doi.org/10.1016/j.gca.2016.03.039
0016-7037/

implying that their mantle sources may be heterogeneous in major element compositions and lithology (e.g., Hauri, 1996; Abouchami, 2007; Jackson and Dasgupta, 2008; Dasgupta et al., 2010). For example, tholeiitic OIBs form a positive CaO/Al_2O_3 vs. $^{206}Pb/^{204}Pb$ trend (Figs. 1 and 2 of Jackson and Dasgupta, 2008). A similar trend is found in Hawaiian tholeiitic lavas, with the magnitude of CaO/Al_2O_3 variation in Hawaiian tholeiites about half of that shown in global OIBs (Abouchami, 2007; Fig. 10 of Jackson et al., 2012). The correlations between major element compositions and isotope ratios have been used to argue for a mafic component in generating OIBs. We are interested in the role of mafic components in the petrogenesis of OIBs, their effects on trace elements, and how the mafic components are sampled.

As one of the best defined hotspot tracks, Hawaiian volcanism is thought to be produced by a mantle plume which rises from the deep mantle (Wilson, 1963), probably from the core-mantle boundary (e.g., Brandon et al., 1999; Humayun et al., 2004; Montelli et al., 2004). Hence, the role of a recycled mafic lithology in the petrogenesis of Hawaiian lavas has great implications to mantle dynamics (e.g., Hofmann and White, 1982). The ages and the amounts of the recycled mafic components inferred in the mantle sources of Hawaiian lavas provide important constraints on the scale and the timing of mantle convection (e.g., Lassiter and Hauri, 1998; Sobolev et al., 2005, 2007). The ubiquitously high Fe/Mn observed in Hawaiian lavas has been interpreted as either addition of Fe by chemical interactions at the core-mantle boundary (Humayun et al., 2004; Huang et al., 2007) or the retention of Mn in the recycled eclogitic crust (Sobolev et al., 2007). Mauna Kea volcano at Hawaii (Fig. 1) is one of the best studied intra-plate oceanic volcanoes (e.g., Blichert-Toft et al., 2003; Eisele et al., 2003; Huang and Frey, 2003; Kurz et al., 2004; Rhodes and Vollinger, 2004; Stolper et al., 2004; Bryce et al., 2005; Blichert-Toft and Albarède, 2009; Rhodes et al., 2012; Nobre Silva et al., 2013), because its shield was drilled and cored by the Hawaii Scientific Drilling Project (HSDP), a 1-km pilot hole (HSDP-1) drilled in 1996 followed by a 3-km hole (HSDP-2) drilled in 1999 and deepened by another 400 m in 2005 (Stolper et al., 1996, 2009; Garcia et al., 2007). The drill cores provide old tholeiitic lavas of this Hawaiian volcano that are not exposed on the surface of the volcano. Although the ages of tholeiitic basalt forming Hawaiian shields are difficult to determine (Jourdan et al., 2012), the relative ages of each lava flow recovered from the drill holes are well constrained. HSDP tholeiitic basalt inferred to be from shield of Mauna Kea define three compositional groups, high-SiO_2, low-SiO_2 and high-CaO (Fig. 2a, b) that bear on the relative roles of peridotite and pyroxenite in generating Hawaiian shield lavas (e.g., Sobolev et al., 2005, 2007; Herzberg, 2006, 2011; Putirka et al., 2011; Rhodes et al., 2012). In this paper we focus on the high-CaO group, which represent one compositional endmember at Mauna Kea and were less studied compared to other HSDP lavas because they were not included in the HSDP-2 reference suite samples selected for study (Rhodes and Vollinger, 2004). This group was first recognized by Stolper et al. (2004), who reported seven volcanic glasses in the HSDP-2

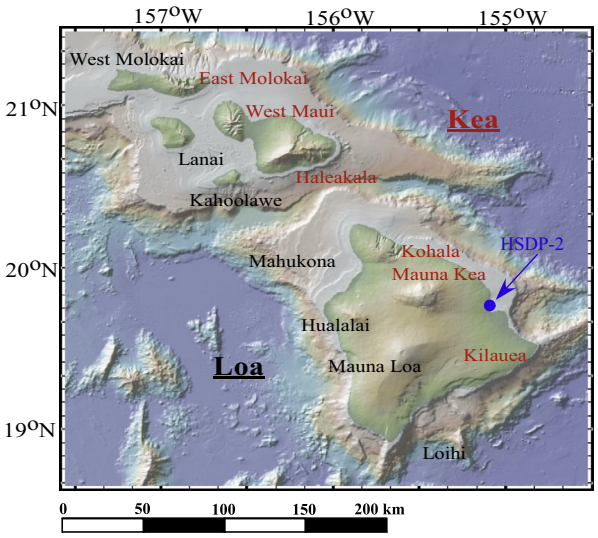

Fig. 1. Map shows Hawaiian volcanoes and the location of the Hawaii Scientific Drilling Project (HSDP-2) drill site.

drill core at the depth interval of 1765–1810 mbsl having the highest CaO contents at a given MgO content among all HSDP-2 glasses. This group was originally referred to as the CaO-K_2O-rich group by Stolper et al. (2004), and then as high-CaO group by Rhodes et al. (2012). Based on the MgO–CaO relationship, Herzberg (2006) argued that the primary magmas of high-CaO group glasses are partial melts of peridotite, and concluded that the primary magmas of all other HSDP-2 Mauna Kea lavas represent partial melts of pyroxenites. Rhodes et al. (2012) re-sampled the 1765–1810 mbsl interval of the HSDP-2 drill core, and recovered twenty-four whole rock samples. They found that whole rocks and glasses share the same distinctive geochemical signatures, such as high CaO content.

Mauna Kea high-CaO group lavas represent the high-CaO, low-SiO_2 endmember of the compositional spectrum shown by Hawaiian tholeiites (Stolper et al., 2004; Rhodes et al., 2012; Fig. 2). In detail, some Loihi alkalic lavas also have similar high CaO content at a given MgO content (e.g., Garcia et al., 1993, 1995, 1998). Analytical work that has been performed on this group of lavas includes: (1) major and some trace element contents of twenty-four whole rocks by XRF (Rhodes et al., 2012); (2) major element contents of seven glasses by electron microprobe (Stolper et al., 2004); and (3) lithophile element abundances of these seven high-CaO glasses by laser ablation inductively coupled plasma mass spectrometry (LA-ICP-MS) (Rhodes et al., 2012). HSDP-2 high-CaO lavas have higher abundances of highly incompatible elements compared to other HSDP tholeiites; consequently, Rhodes et al. (2012) suggested that high-CaO lavas were generated by lower degrees of partial melting. Here, we report elemental abundances of first-row transition metals and precise Fe/Mn determined *in situ* by LA-ICP-MS on these seven HSDP high-CaO glasses. With these data, we test whether the high Fe/Mn is a common feature of all Hawaiian shield-stage lavas (Humayun et al., 2004;

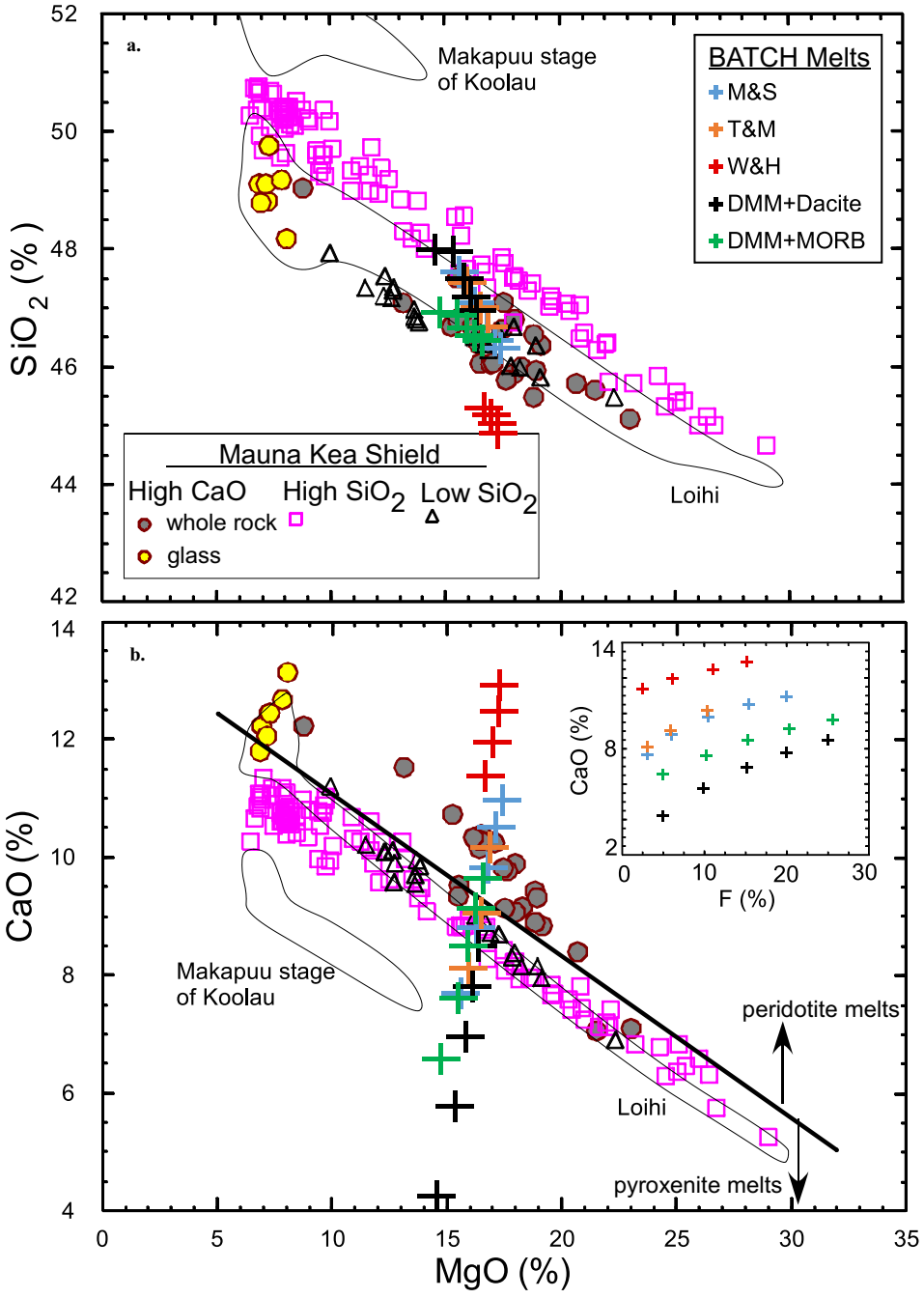

Fig. 2. MgO vs. SiO_2, CaO (all in wt%), V, Sc, Nb, Zr, Y and CaO/Al_2O_3 for Mauna Kea tholeiites recovered from HSDP-2. Fields for Makapuu-stage of Koolau and Loihi are shown in Panels a and b for comparison. The steep MgO-SiO_2 and –CaO trend of high-CaO glasses might infer minor clinopyroxene fractionation (Stolper et al., 2004). In Panel b, the line separating the partial melts of peridotite from partial melts of garnet pyroxenite is taken from Herzberg (2006). Also in Panels a and b are the melt compositions saturated with all four phases of garnet peridotite calculated using BATCH program (Longhi, 2002 version data 1/09). Specifically, five different starting compositions are used (see Tables 2 and S1 for details). Inset in Panel b shows the melt CaO content as a function of degree of partial melting. Panel d shows that the large CaO/Al_2O_3 variation in High-CaO whole rocks is caused by alteration, and olivine is the dominant crystal phase in High-CaO lavas. The CaO/Al_2O_3 variations in Hawaiian tholeiites and global OIBs are shown for comparison (Jackson and Dasgupta, 2008; Jackson et al., 2012). Fields for Makapuu-stage of Koolau lavas and EPR MORB (downloaded data from PetDB http://www.earthchem.org/petdb) are shown in Panel f for comparison. HSDP-2 High-CaO glasses fall well within the MORB field. Data are from Frey and Clague (1983), Garcia et al., 1993, 1995, 1998); Norman and Garcia (1999), Huang and Frey (2003), Rhodes and Vollinger (2004), Stolper et al. (2004), Rhodes et al. (2012) and this study.

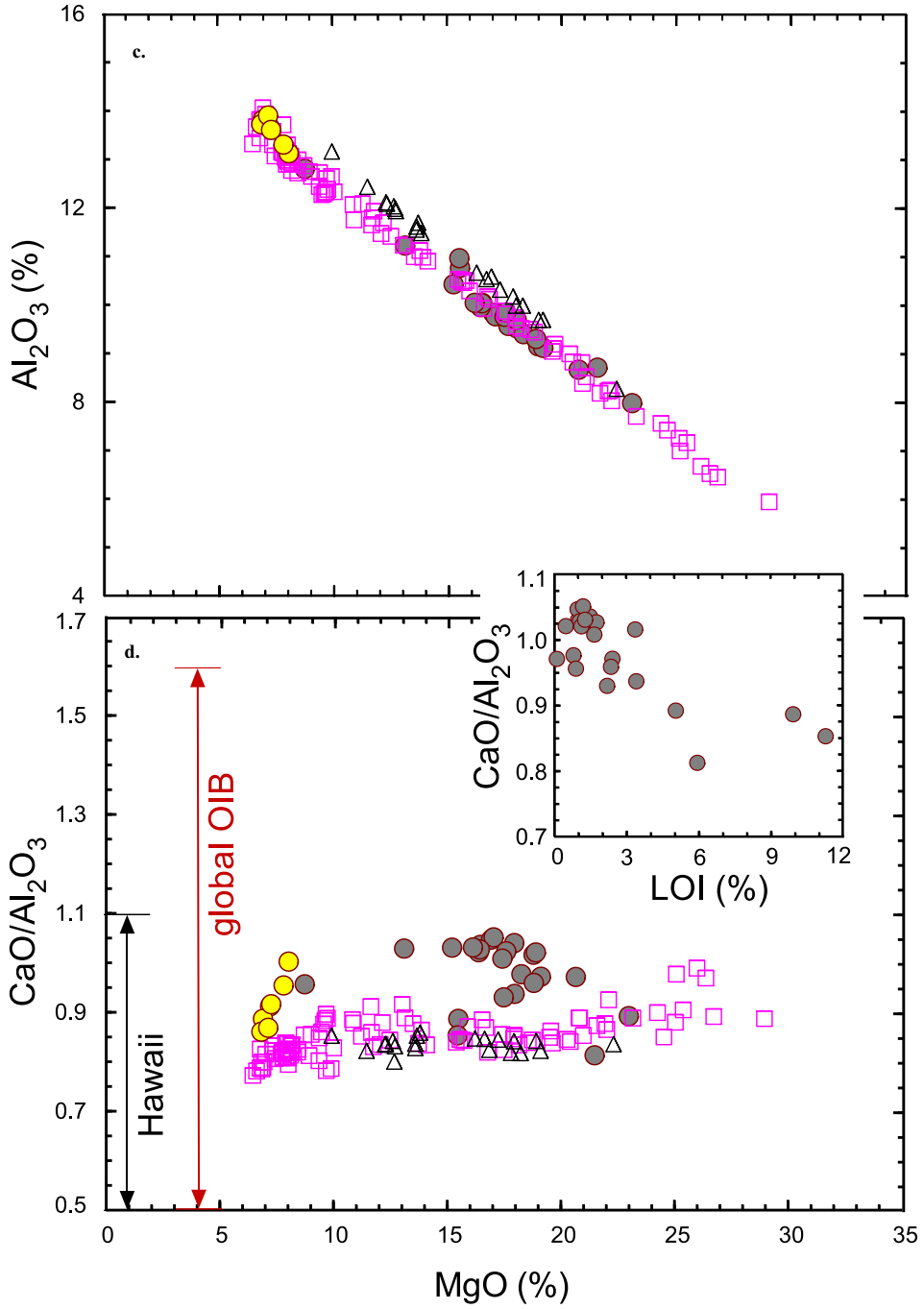

Fig 2. *(continued)*

Huang et al., 2007), and explore the role of pyroxenite in forming the high-CaO lavas.

2. ANALYTICAL PROCEDURES

HSDP-2 high-CaO glasses, mounted and analyzed for major elements by electron probe at University of Hawaii and California Institute of Technology (Stolper et al., 2004; Table 1), were analyzed by LA-ICP-MS using a Finnigan Element™ ICP-MS with a New Wave UP213 (213 nm UV) laser ablation system at Florida State University (Humayun et al., 2007). Two separate series of measurements were performed, the first with the Element™ in low resolution ($R = 400$) for Fe/Mn and the second for elemental abundances with the Element™ in medium resolution ($R = 4000$). The LA-ICP-MS Fe/Mn analyses were conducted in spot mode with 100 μm spot size, 10 Hz repetition rate, ~1.1 mJ laser energy output, and a 30-s ablation time for each spot. The peaks ^{55}Mn, ^{57}Fe, and ^{60}Ni, were collected at low resolution with 200 mass scans per spot. Since

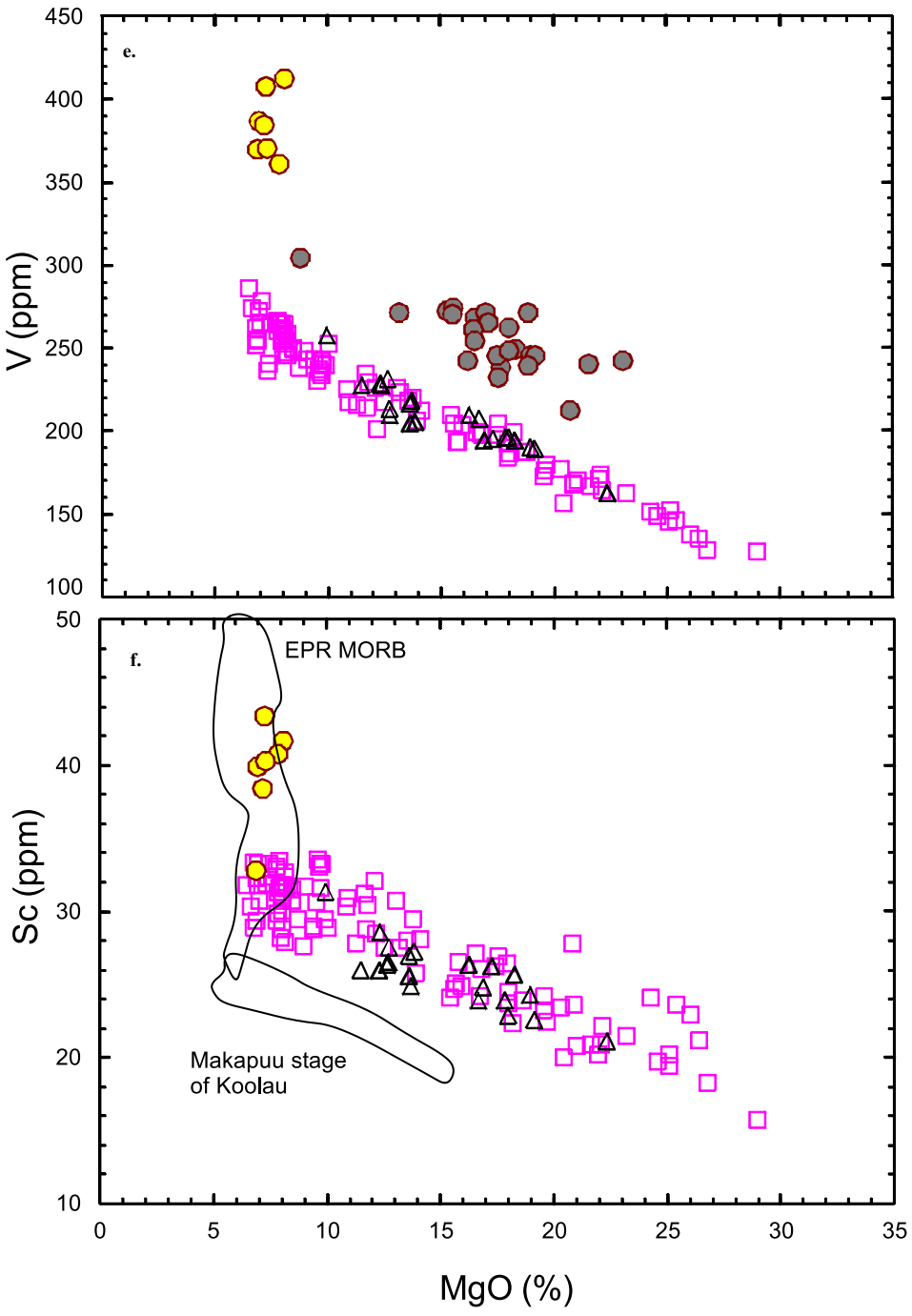

Fig 2. *(continued)*

there are olivine microphenocrysts in the glasses, with distinctly higher Fe/Mn, ^{60}Ni was monitored to reject analyses that accidentally ablated olivine microphenocrysts. The polyatomic interferences, ArN^+ and ArO^+, were corrected by measuring their intensities with the laser off, and these interference corrections on ^{55}Mn and ^{57}Fe were less than 0.7% throughout the analyses. Each reference glass or sample glass was analyzed with multiple spots (2–9). The measured ^{57}Fe/^{55}Mn intensity ratios were then converted to Fe/Mn abundance ratios using the MPI-DING glasses KL2-G and ML3B-G as standard samples (Jochum et al., 2006). The measured Fe/Mn and elemental abundances are in Table 1. It is important to mention that the measured Fe/Mn (65.4 ± 0.4, 2σ, $n = 9$) in BHVO-2 g glass by LA-ICP-MS is within analytical error of Fe/Mn (65.3 ± 0.4, 2σ, $n = 6$) in BHVO-2 powder measured by solution ICP-MS (Huang et al., 2007).

For elemental abundances, the UP213 laser ablation system was used in line mode with 65 μm spot size, scanned over the sample surface at a rate of 10 μm/s, 10 Hz laser

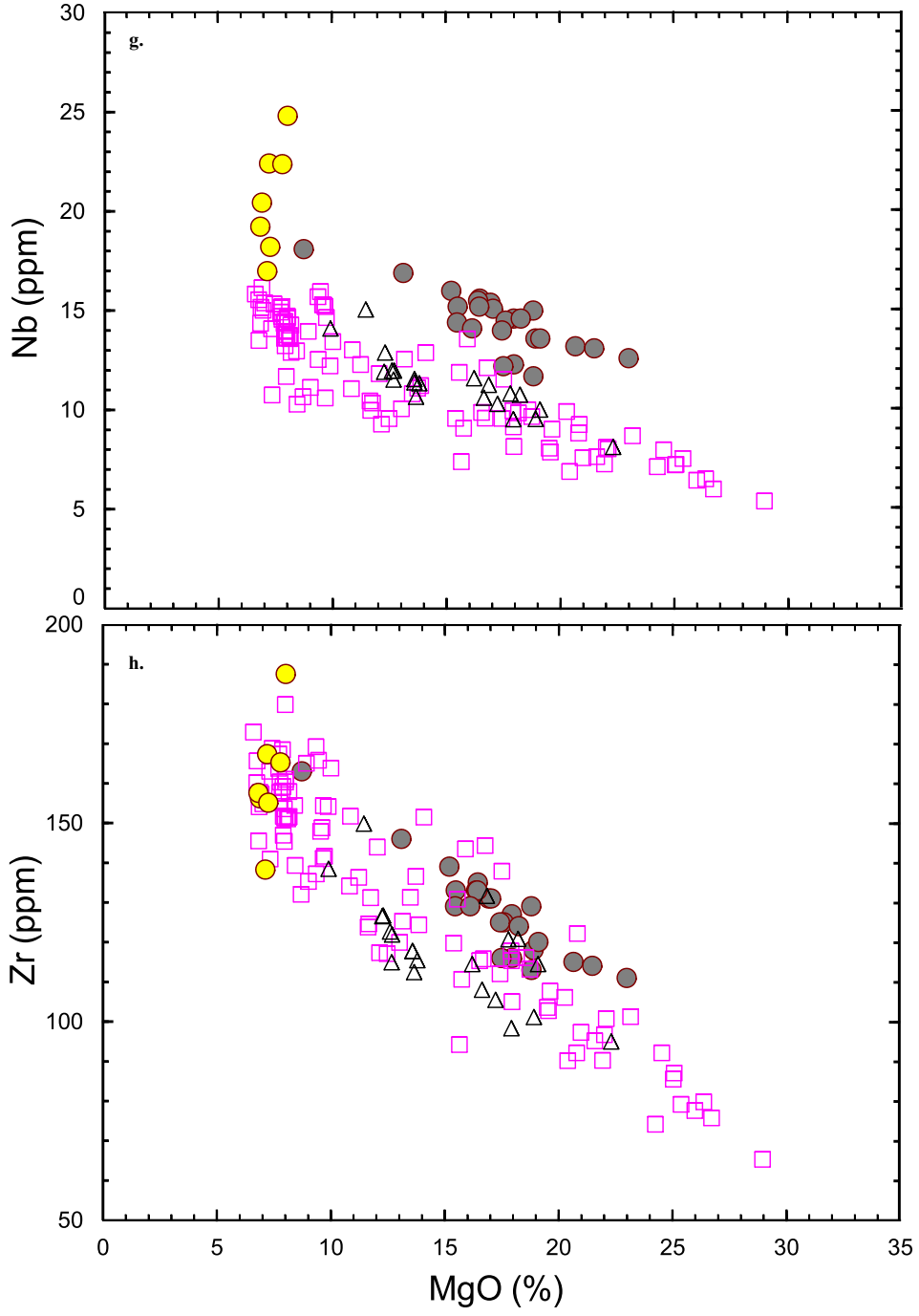

Fig 2. *(continued)*

repetition rate, and 0.4–0.6 mJ energy output. Elemental analyses were conducted in medium resolution ($R = 4000$) to resolve numerous molecular isobaric interferences, monitoring the peaks ^{24}Mg, ^{27}Al, ^{28}Si, ^{44}Ca, ^{45}Sc, ^{47}Ti, ^{51}V, ^{52}Cr, ^{55}Mn, ^{56}Fe, ^{59}Co, ^{60}Ni, ^{63}Cu, ^{66}Zn, ^{69}Ga, and ^{74}Ge. Intensity ratios with respect to ^{28}Si were converted to elemental ratios with respect to SiO_2 using the MPI-DING glass standards GOR128-G, KL2-G, ML3B-G and T1-G (Jochum et al., 2006) for calibration, except for Ge, which was calibrated using NIST SRM 612 (Pearce et al., 1997). The sum of the electron probe abundances of Na_2O, K_2O and P_2O_5 (not determined by this laser ablation method) were 3.2 ± 0.4 wt% (2σ) for all seven glasses (Stolper et al., 2004), so other major element (MgO, Al_2O_3, SiO_2, CaO, TiO_2, MnO and FeO_T) contents for each glass were then determined by summing all measured oxides to 96.8%. The presence of olivine and spinel microphenocrysts was detected by examining each analysis in time-resolved mode, and the high MgO, Cr, and Ni regions were deleted from the glass analysis. However, a small residual contam-

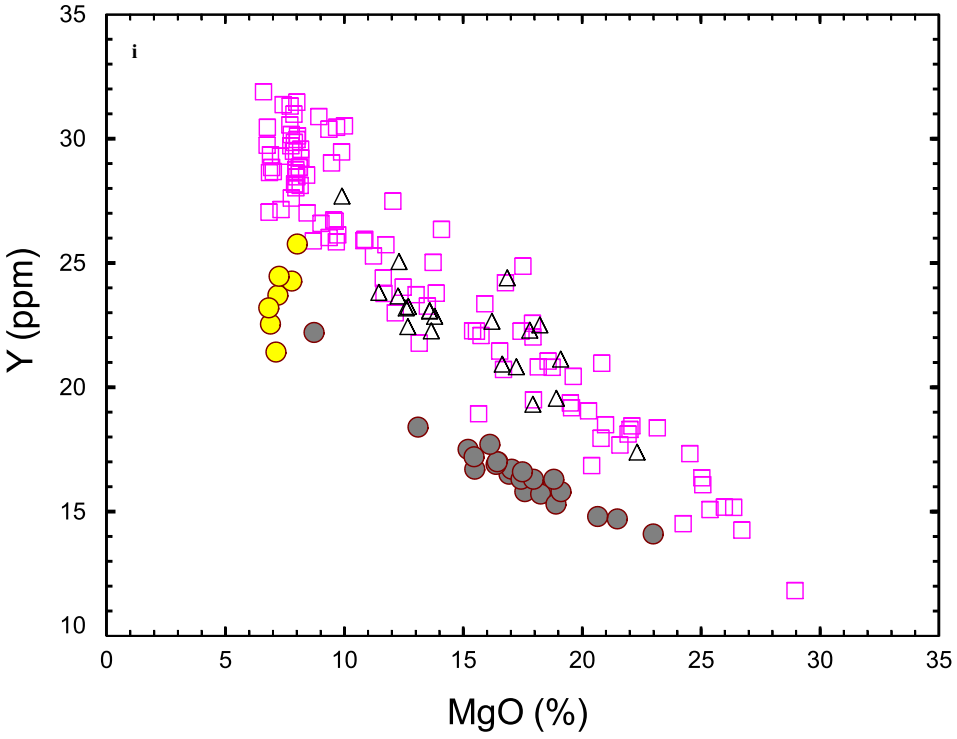

Fig 2. *(continued)*

ination of each analysis by olivine was unavoidable, so that our glass data are biased towards higher MgO contents than the e-probe measurements. The USGS standards BCR-2g and BHVO-2g were analyzed as unknowns and are reported in Table 1.

3. RESULTS

The relative differences between contents of seven major elements (MgO, Al_2O_3, SiO_2, CaO, TiO_2, MnO and FeO_T) in HSDP-2 high-CaO glasses determined by our LA-ICP-MS technique and that by e-probe are less than 15%, except for MgO content in SR689 which differs by 20% (Table 1). The large discrepancy in MgO reflects the presence of olivine microphenocrysts that were accidentally ablated during laser ablation and were not able to be removed. This shows the potential that LA-ICP-MS technique may be used as an alternative analytical method determining major element compositions of glasses, which are traditionally determined using e-probe. In our following discussion, major element contents determined by e-probe (Stolper et al., 2004) are used.

Lithophile element abundances of HSDP-2 high-CaO glasses have been reported by Rhodes et al. (2012). Here we report the first row transitional metal abundances determined by LA-ICP-MS (Table 1). First row transitional metal abundances in USGS standards BCR-2g and BHVO-2g determined as unknowns in this study agree within errors with the accepted values from GeoREM, with Ge being the only exception.

The trace element abundances of HSDP-2 high-CaO lavas have been characterized by Rhodes et al. (2012) and our new LA-ICP-MS data on glasses (Table 1). At a given MgO content, compared to HSDP-2 high- and low-SiO_2 lavas, high-CaO lavas have higher abundances of the most incompatible elements, such as Nb, similar abundances of moderately incompatible elements, such as Zr, and higher abundances of the least incompatible elements, such as Sc and V (Fig. 2). Olivine is the only major phenocryst phase in HSDP-2 high CaO lavas (Rhodes et al., 2012), so that the high Sc and V abundances in high-CaO lavas are not the result of clinopyroxene accumulation.

HSDP-2 high-CaO glasses have Fe/Mn >63 and plot at the low-MgO end of the olivine-control trend defined by Kilauea lavas (Fig. 3). Also plotting on this trend are our measurements of a Kilauea sample, USGS standard BHVO-2g, run concurrently with the HSDP-2 high-CaO glasses. For comparison, MORB and Icelandic lavas (Qin and Humayun, 2008) plot well below this trend (Fig. 3). Despite the large isotopic and compositional variations in Hawaiian shield lavas (e.g., Frey et al., 1994; Stolper et al., 2004; Fig. 2), lavas with endmember compositions, including Makapuu-stage Koolau lavas (high-SiO_2 and low-CaO end) and Mauna Kea HSDP-2 high-CaO glasses (low-SiO_2 and high-CaO end), have essentially the same Fe/Mn.

4. DISCUSSION

4.1. Is CaO content a useful criterion to distinguish between partial melts of pyroxenite and peridotite?

On a global scale, major element contents, after correction for olivine fractionation effect, of OIBs are correlated

Table 1
Major and trace element contents and Fe/Mn in HSDP-2 high-CaO group glasses.

	SR684	SR686	SR689	SR697	SR698	SR699	SR700	Uncertainty	BHVO-2g	BHVO-2g GeoREM	BCR-2g	BCR-2g GeoREM
Depth (mbsl[a])	1766.5	1771.5	1779.4	1800.1	1802.5	1805.7	1807.6					
Unit	248	248	248	254	255	256	256					
e-probe analyses (wt%) from Stolper et al. (2004)												
SiO_2	48.19	48.83	48.80	49.12	49.12	49.19	49.77					
TiO_2	2.63	2.62	2.70	2.74	2.60	2.43	2.55					
Al_2O_3	13.12	13.65	13.81	13.72	13.9	13.3	13.6					
FeO_T	11.03	11.29	11.58	11.71	11.14	10.83	10.94					
MnO	0.18	0.17	0.18	0.20								
MgO	8.03	7.21	6.90	6.83	7.13	7.8	7.26					
CaO	13.15	12.45	12.24	11.81	12.07	12.69	12.46					
Na_2O	2.27	2.36	2.37	2.40	2.31	2.13	2.29					
K_2O	0.74	0.72	0.73	0.77	0.66	0.56	0.60					
P_2O_5	0.31	0.25	0.27	0.29	0.25	0.19	0.20					
Total	99.65	99.55	99.58	99.59	99.18	99.12	99.67					
	CalTech	CalTech	UHawaii	UHawaii	UHawaii	UHawaii	UHawaii					
LA-ICP-MS analyses												
Major element content (%)												
SiO_2	47.6	48.2	49.0	49.5	48.4	49.6	49.4	0.3				
TiO_2	2.73	2.85	2.56	2.56	2.80	2.45	2.57	0.03				
Al_2O_3	12.3	12.6	12.5	14.3	13.4	12.6	12.8	0.2				
FeO_T	11.4	11.2	10.8	10.4	11.0	10.3	10.7	0.2				
MnO	0.176	0.169	0.171	0.161	0.171	0.164	0.169	0.003				
MgO	8.71	7.65	8.30	6.64	7.21	8.18	7.73	0.09				
CaO	13.9	14.2	13.6	13.3	13.8	13.4	13.5	0.2				
Trace element abundance (ppm)												
Sc	41.7	43.4	40.0	32.9	38.5	40.8	40.4	0.9	35.1	33 ± 2	35.7	33 ± 2
V	413	408	387	370	385	362	371	7	303	308 ± 19	414	425 ± 18
Cr	370	255	330	366	413	642	391	21	311	293 ± 12	16	17 ± 2
Co	48.6	46.0	46.7	40.7	42.8	45.4	44.6	0.8	44.0	44 ± 2	38.0	38 ± 2
Ni	200	138	150	103	98	135	115	5	126	116 ± 7	9	13 ± 2
Cu	181	165	152	154	179	169	161	4	121	127 ± 11	15	21 ± 5
Zn	177	116	104	97	257	210	153	6	98	102 ± 6	136	125 ± 5
Ga	21.3	20.0	19.8	20.5	20.3	19.4	19.0	0.5	19.9	22 ± 3	20.9	23 ± 1
Ge	1.1	1.2	1.2	1.2	1.1	1.1	1.2	0.1	1.3	1.6 ± 0.1	1.3	1.5 ± 0.1
Fe/Mn		63.8	63.7	63.5	63.9	64.4	63.5		65.4	67	63.2	62
2-stdev, relative		1.3%	0.8%	1.3%	1.9%	1.4%	1.0%		0.6%		1.9%	
n		5	4	4	5	5	6		9		2	

[a] mbsl: meters below sea level.

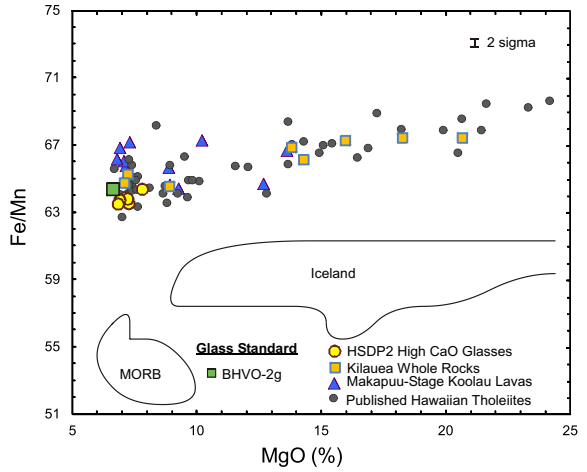

Fig. 3. MgO (wt%) vs. Fe/Mn (on a weight basis) in HSDP-2 high-CaO glasses. Hawaiian basaltic reference glass BHVO-2g (from Kilauea) is also shown. 2σ error bar is estimated based on 9 LA-ICP-MS analyses of BHVO-2g. Published data of Hawaiian shield lavas (Humayun et al., 2004; Huang et al., 2007), and fields for MORB (from all ocean basins) and for Icelandic lavas (Qin and Humayun, 2008) are shown for comparison. Hawaiian data are filtered for alteration using the criteria of $1.3 < K_2O/P_2O_5 < 2.0$ (see Huang et al., 2007 for discussion).

with their radiogenic isotope ratios (e.g., Jackson and Dasgupta, 2008). For example, OIBs form a positive CaO/Al_2O_3 vs. $^{206}Pb/^{204}Pb$ trend. On a local scale, Hawaiian lavas also form a positive CaO/Al_2O_3 vs. $^{206}Pb/^{204}Pb$ trend (Abouchami, 2007; Fig. 10 of Jackson et al., 2012). CaO/Al_2O_3 variation in Hawaiian lavas is about half of that in global OIBs, and HSDP-2 high-CaO lavas define the high-CaO/Al_2O_3 end at Hawaii (Fig. 2). Rhodes (2016) showed that all Hawaiian shield lavas, after correction for olivine fractionation, have essentially the same Al_2O_3 content. Consequently, the large CaO/Al_2O_3 variation in Hawaiian lavas (Abouchami, 2007; Fig. 10 of Jackson et al., 2012; Fig. 2) reflects CaO variation. Based on the partial melting experiments of peridotite by Walter (1998), Herzberg (2006) proposed that CaO content at a given MgO content is a useful parameter distinguishing between partial melts of peridotite and garnet pyroxenite, with partial melts of peridotite having higher CaO content than partial melts of garnet pyroxenite (Fig. 2b). Using this CaO criterion, most Hawaiian shield lavas have CaO content too low to be partial melts of peridotite, and only a small group of Loihi lavas and HSDP-2 high-CaO lavas from Mauna Kea represent partial melts of peridotite (Herzberg, 2006; Fig. 2b). The low CaO contents in most Hawaiian shield lavas then represent contribution from partial melts of garnet pyroxenite. This inference is important in estimating the amount of recycled mafic component in the mantle source of Hawaiian lavas, presumably the Hawaiian plume. However, recent partial melting experiments in CO_2-free systems showed that low-degree partial melts of garnet peridotite could have low CaO contents (Balta et al., 2011; Davis et al., 2013). Furthermore, Herzberg et al. (2014) showed that partial melts of a peridotite fertilized by a dacite melt (low CaO) from eclogite also have low CaO contents.

In order to further test whether CaO content in melt can be used to distinguish between partial melting of peridotite and pyroxenite, a series of calculations have been run using the BATCH program (Longhi, 2002 version Date 1/09) at CalTech by M. Baker (Tables 2 and S1). Specifically, five peridotite compositions (Table S1) have been used to test the effect of source heterogeneity: primitive mantle compositions from McDonough and Sun (1995) and Taylor and McLennan (2009), a depleted mantle composition (Workman and Hart, 2005), a mixture of 80% depleted mantle and 20% average MORB (Gale et al., 2013), and a mixture of 80% depleted mantle and 20% dacite magma (Run A190, Pertermann and Hirschmann, 2003). Partial melts that are saturated with all four phases (olivine, orthopyroxene, clinopyroxene and garnet) are compared with HSDP-2 tholeiites in plots of MgO vs. SiO_2 and CaO (Fig. 2a, b). BATCH calculations show that CaO contents in 4-phase saturated melts are controlled by both degrees of partial melting (Fig. 2b; Walter, 1998), and source composition, and they plot below and above the Herzberg-Asimow line in a diagram of MgO vs. CaO (Fig. 2b). Consequently, as suggested by Herzberg et al. (2014), melt CaO content may not be a reliable criterion for distinguishing partial melts of peridotite from partial melts of pyroxenite. However, these results do not preclude the interpretation that HSDP-2 high-CaO lavas are partial melts of peridotite. Following Stolper et al. (2004), both HSDP-2 low-SiO_2 and high-CaO lavas could be partial melts of peridotites, but the high-SiO_2 lavas cannot be directly generated from peridotite. Specifically, HSDP-2 low-SiO_2 and high-CaO parental magmas match well with experimental partial melts from peridotites generated under ~3 GPa (see Fig. 13 of Stolper et al., 2004).

Programs such as BATCH (Longhi, 2002) and pMELTs (Ghiorso et al., 2002) are widely used to constrain phase relationship during partial melting and crystallization. We used the BATCH program to show the effects of partial melting degree and source composition on the CaO contents of partial melts; however, it may be difficult to use the BATCH program to investigate the small compositional differences between HSDP-2 high-CaO and low-SiO_2 lavas. This is because these programs are calibrated against high-P, high-T partial melting experiments in which the uncertainty of absolute temperature is on the order of ±10 °C (e.g., Walter, 1998; Keshav et al., 2004). In contrast, the temperature interval between the solidus and the liquidus of a volatile-free garnet peridotite is ~100 °C, and the temperature interval in which all five phases co-exist is much smaller (e.g., Walter, 1998). In the following sections, we will use trace element contents to address the role of pyroxenite in the petrogenesis of HSDP-2 high-CaO lavas.

4.2. Constraints from trace elements: a role of mafic cumulate in the petrogenesis of high-CaO lavas

4.2.1. Observations

As typical of Hawaiian shield tholeiites, HSDP-2 lavas form negative trends in plots of MgO vs. incompatible

Table 2
Phase proportions of basaltic liquids saturated with four phases.

Run #	T (°C)	P (GPa)	liq	oliv	opx	cpx	gt
M&S 0.98	1549	3	0.03	0.58	0.05	0.25	0.09
M&S 0.95	1556	3	0.06	0.57	0.06	0.23	0.07
M&S 0.90	1561	3	0.10	0.57	0.09	0.18	0.05
M&S 0.85	1565	3	0.15	0.56	0.12	0.13	0.03
M&S 0.80	1568	3	0.20	0.55	0.16	0.07	0.02
M&S + 5% mafic cumulate	1549	3	0.09	0.56	0.01	0.26	0.09
M&S + 5% mafic cumulate	1556	3	0.12	0.56	0.03	0.23	0.07
M&S + 10% mafic cumulate	1556	3	0.19	0.54	0.00	0.22	0.06
T&M 0.98	1554	3	0.03	0.56	0.17	0.19	0.04
T&M 0.95	1560	3	0.06	0.56	0.19	0.17	0.03
T&M 0.90	1562	3	0.10	0.55	0.22	0.11	0.01
T&M 0.85	1552	3	0.15	0.55	0.27	0.03	0.00
T&M 0.80	1580	3	0.20	0.54	0.26	0.00	0.00
W&H 0.98	1546	3	0.02	0.59	0.12	0.20	0.07
W&H 0.95	1554	3	0.06	0.59	0.15	0.16	0.05
W&H 0.90	1560	3	0.11	0.58	0.19	0.09	0.03
W&H 0.85	1560	3	0.15	0.57	0.23	0.03	0.01
W&H 0.80	1579	3	0.20	0.56	0.24	0.00	0.00
W&H + 5% mafic cumulate	1546	3	0.10	0.56	0.12	0.17	0.06
W&H + 5% mafic cumulate	1554	3	0.13	0.56	0.15	0.12	0.04
W&H + 10% mafic cumulate	1546	3	0.17	0.53	0.11	0.14	0.05
W&H + 10% mafic cumulate	1554	3	0.20	0.53	0.15	0.08	0.03
W&H + partial melt 0.95	1561	3	0.05	0.41	0.04	0.34	0.17
W&H + partial melt 0.90	1561	3	0.10	0.40	0.04	0.30	0.15
W&H + partial melt 0.85	1560	3	0.15	0.39	0.07	0.26	0.12
W&H + partial melt 0.80	1560	3	0.20	0.39	0.10	0.21	0.10
W&H + partial melt 0.80	1560	3	0.25	0.38	0.14	0.16	0.07
W&H + avg MORB 0.95	1540	3	0.05	0.43	0.00	0.38	0.14
W&H + avg MORB 0.90	1548	3	0.10	0.43	0.02	0.34	0.11
W&H + avg MORB 0.85	1551	3	0.15	0.42	0.05	0.29	0.09
W&H + avg MORB 0.80	1554	3	0.20	0.42	0.08	0.24	0.07
W&H + avg MORB 0.75	1557	3	0.26	0.41	0.11	0.18	0.04

Starting materials: (all compositions are in Table S1).
M&S: Primitive mantle from McDonough and Sun (1995).
T&M: Primitive mantle from Taylor and McLennan (2009).
W&H: Depleted mantle from Workman and Hart (2005).
W&H + partial melt: 80% depleted mantle (Workman and Hart, 2005) + 20% dacite magma (A190, Pertermann and Hirschmann, 2003).
W&H + MORB: 80% depleted mantle (Workman and Hart, 2005) + 20% average MORB (Gale et al., 2013).
Mafic cumulate: delaminated mafic cumulate from Jagoutz and Schmidt (2013).
Temperatures are calculated using the olivine-melt thermometer of Ford et al. (1983), with an error on the order of ±10 °C. Such values are only used here as a reference to distinguish between different model calculations.

elements (Fig. 2), reflecting olivine control. Since we are interested in mantle processes, we removed the effects of olivine fractionation and accumulation on trace element abundances by calculating their abundances at MgO = 16 wt% using a simple MgO-trace element correlation (Fig. 2). This value is selected because most primitive melts that are saturated with 4-phase peridotites have MgO content around 16% (see results of melting models using BATCH in Fig. 2a, b). As shown in Figs. 4a and S1, average HSDP-2 high-SiO_2 and low-SiO_2 lavas have almost the same trace element patterns. This is a surprising result because HSDP-2 high- and low-SiO_2 lavas are distinctively different in SiO_2 content (Fig. 2a) and isotopic compositions (e.g., Blichert-Toft et al., 2003; Eisele et al., 2003; Kurz et al., 2004; Bryce et al., 2005). High-CaO lavas are different from high- and low-SiO_2 lavas: If normalized to the average composition of low-SiO_2 lavas, high-CaO lavas form a U-shaped pattern, i.e., relatively high abundances in both the most and the least incompatible elements (Fig. 4b). High-CaO whole rocks with MgO >10% have higher abundances of Nb and V than high- and low-SiO_2 lavas, confirming that the U-shaped trace element pattern of High-CaO lavas when normalized to low-SiO_2 lavas is not an artifact of crystal fractionation correction.

Here we will investigate the possible petrogenetic relationship between HSDP-2 high-CaO and low-SiO_2 lavas. The over-all enrichment of highly incompatible elements in high-CaO lavas compared to low-SiO_2 lavas implies a

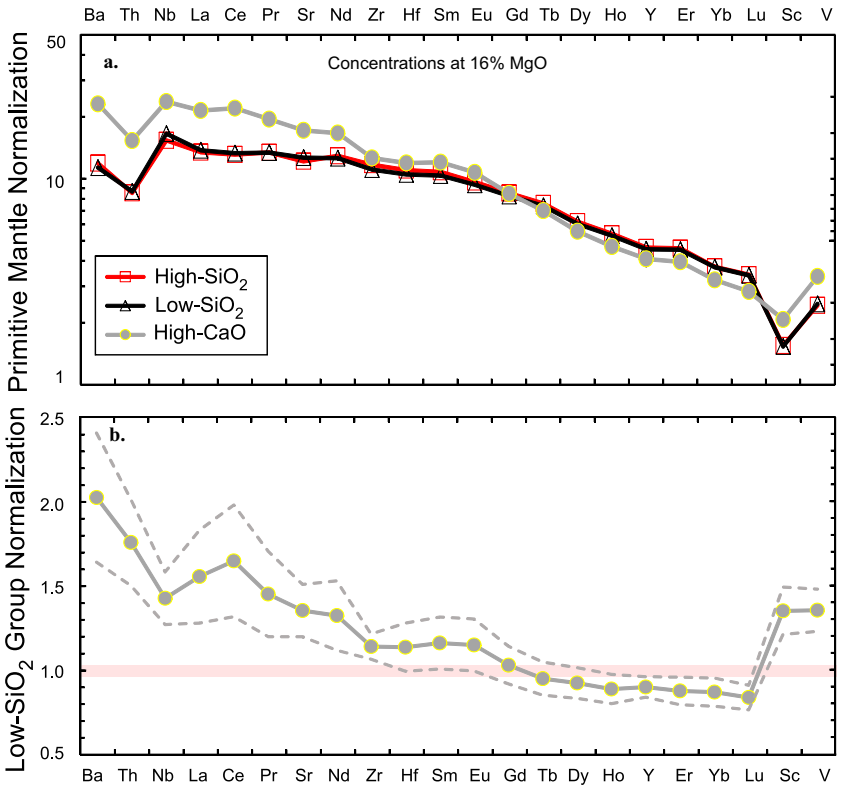

Fig. 4. (a) Average trace element patterns, normalized to primitive mantle (McDonough and Sun, 1995), of three HSDP-2 tholeiitic groups: high-SiO_2, low-SiO_2, and high-CaO. Specifically, all lavas compositions are normalized to MgO = 16% using a simple MgO-trace element correlation (Fig. 2) to remove the effect of olivine fractionation/accumulation. (b) Average composition of high-CaO lavas at MgO = 16% normalized to that of low-SiO_2 lavas. In this panel, high-CaO lavas form a U-shape pattern. The dashed lines outline the 1-sigma variation of the average composition of high-CaO lavas.

lower degree of partial melting of the same mantle source for the high-CaO and low-SiO_2 lavas (Rhodes et al., 2012). However, a lower extent of melting alone does not explain the Sc and V enrichment in high-CaO lavas because their abundances are insensitive to the degrees of partial melting (see Section 4.2.2; Figs. 5a; S4a). This is because Sc and V have high clinopyroxene/melt and garnet/melt partition coefficients (e.g., Hart and Dunn, 1993; Adam and Green, 2006; Hill et al., 2011; Fig. S2), and both clinopyroxene and garnet are preferentially melted during partial melting (e.g., Walter, 1998); consequently, the bulk partition coefficients of the melt (Ps) for Sc and V are close to one. In addition, a lower extent of partial melting also leads to lower CaO content (inset in Fig. 2b), which is inconsistent with the higher CaO content in high-CaO lavas. An alternative explanation is that Sc and V enrichment of high-CaO lavas reflects a source signature. A possible process for enriching a source in Sc and V is addition of a clinopyroxene-rich cumulate rock to a peridotite. For example, the delaminated mafic cumulates formed under arcs during the formation of andesitic arc crusts are characterized by high Sc and V abundances (Fig. 5d; Jagoutz and Schmidt, 2013). Garnet pyroxenites recovered from Salt Lake Crater at Honolulu Volcanics, Hawaii, represent high-pressure cumulates, and they are also characterized by high Sc and V abundances (Frey, 1980; Bizimis et al., 2005; Sen et al., 2011).

Here we model two endmember scenarios during partially melting a mixture of peridotite and pyroxenite. Because of their different solidus temperatures (e.g., Hirschmann and Stolper, 1996; Keshav et al., 2004; Pertermann et al., 2004), during the upwelling of such mixture, pyroxenite starts to melt deeper, and peridotite starts to melt at a shallower depth (Fig. 6). There are two scenarios. In case A, partial melts from pyroxenite and peridotite migrate to the magma chamber separately, and mix with each other in the magma chamber (Fig. 6). We call this scenario "magma-magma mixing". Because of the difference in solidus temperatures, when the peridotite starts to melt, the mafic component (garnet pyroxenite/eclogite) has melted to a much larger degree (e.g., Hirschmann and Stolper, 1996; Keshav et al., 2004; Pertermann et al., 2004).

In case B (Fig. 6), melts from peridotite and pyroxenite mix with each other in the mantle, which leads to a homogeneous melt. Such melt is equilibrated with both peridotite and pyroxenite; consequently, it forces peridotite and pyroxenite to have the same mineral compositions for clinopyroxene and garnet. Adding pyroxenite is then equivalent to partial melting of a homogeneous, fertile (or refertilized) peridotite source (Case B of Fig. 6). This scenario can also be explained using the melt-mantle reaction model proposed by Sobolev et al. (2005). That is, pyroxenite melts at greater depth to a large degree, and such melt reacts with

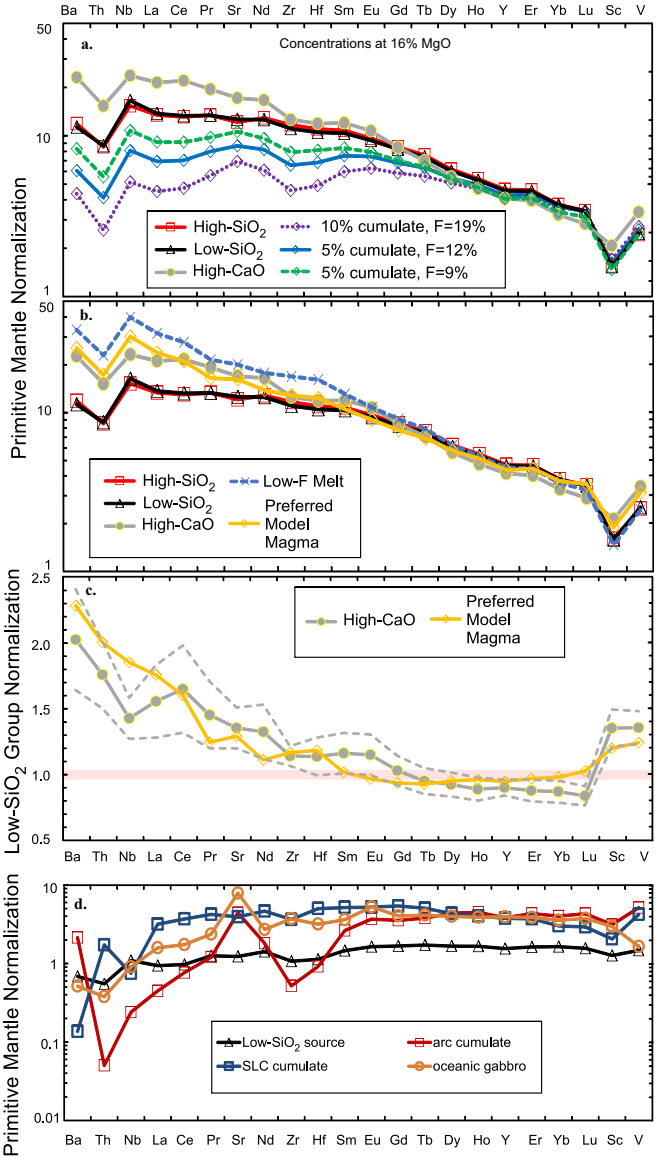

Fig. 5. Average trace element patterns at MgO = 16%, normalized to primitive mantle (McDonough and Sun, 1995), of three HSDP-2 tholeiitic groups: high-SiO_2, low-SiO_2, and high-CaO. In Panel a, three partial melts of fertilized peridotites are shown for comparison. This is the scenario discussed in Section 4.2.2. In Panel b, a lower degree (2%) partial melt of the low-SiO_2 mantle source, and our preferred model, that is a mixture of 75% of this lower degree partial melt and 25% of a mafic cumulate, are shown for comparison. This mixture can reproduce the trace element pattern observed in high-CaO lavas. A linear scale version is shown in Fig. S1a. In Panel c, the average composition of low-SiO_2 lavas is used as the normalization value. In this panel, high-CaO lavas form a U-shaped pattern. The dashed lines outline the 1-sigma variation of the average composition of high-CaO lavas. At this level, the trace element pattern of high-CaO lavas can be reproduced by our preferred model (the scenario discussed in Section 4.2.3). Panel d shows the trace element patterns (normalized to the Primitive Mantle value of McDonough and Sun, 1995) of the mafic cumulate delaminated during the continent formation under the arcs (Jagoutz and Schmidt, 2013), a garnet pyroxenite from Salt Lake Crater, Hawaii (Bizimis et al., 2005; Sen et al., 2011), unaltered oceanic gabbro (Hart et al., 1999), the calculated mantle source of HSDP-2 low-SiO_2 lavas. Since Jagoutz and Schmidt (2013) did not report Sc abundance in the delaminated mafic cumulate, it is calculated using the same mass balance approach specified in Jagoutz and Schmidt (2013). That is, the bulk continental crust is formed after a mafic cumulate is removed from the primitive arc lava. Particularly, a cumulate/crust ratio of 2.34 is used. The bulk continental crust has 21.9 ppm Sc (Rudnick and Gao, 2003). Sc abundance in primitive arc lavas is calculated using V/Sc = 6 (at MgO = 11%) (Fig. 10 of Lee et al., 2005) and a V abundance of 247 ppm (Jagoutz and Schmidt, 2013). The plotted Salt Lake Crater garnet pyroxenite is calculated using 70% clinopyroxene and 30% garnet (Bizimis et al., 2005) and V/Sc of 10.4 (Sen et al., 2011).

peridotite to form a fertilized peridotite. Then this fertilized peridotite partially melts to contribute to a volcano. When pyroxenite is melted to nearly 100%, in contrast to ~50% in the original model by Sobolev et al. (2005), the enriched peridotite would have a composition equivalent to the mixture of pyroxenite and peridotite. We call this scenario "solid–solid mixing". Can these two mixing scenarios be distinguished from each other?

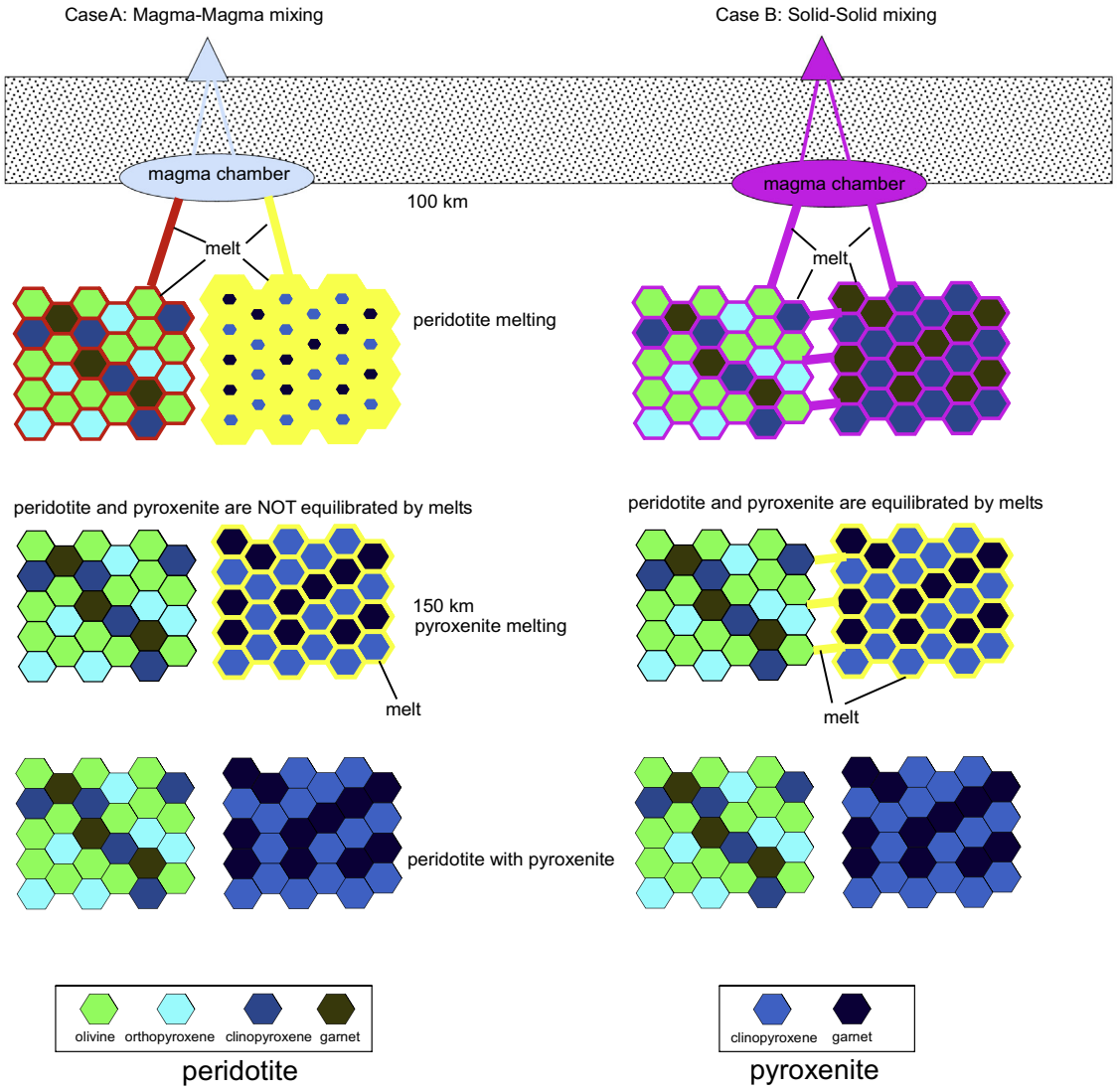

Fig. 6. Cartoons showing the two scenarios of partial melting of a pyroxenite-peridotite mixture. In Case A, pyroxenite and peridotite melt separately at different depths. Their magmas do not mix with each other in the mantle, and make their own way to the magma chamber where they mix and erupt. In case B, pyroxenite melts at greater depth, and its melt wets both pyroxenite and peridotie. That is, a melt phase is in equilibrium with both pyroxenite and peridotie. This is equivalent to partial melting a peridotite fertilized by a pyroxenite. See text for details.

4.2.2. A role of mafic cumulate: solid–solid mixing

In this scenario, mixing of the mafic component with peridotite creates a fertilized peridotite, with relatively high Sc and V abundances, and high modal abundances of clinopyroxene and garnet. Consequently, partial melts of this fertilized peridotite may not have high abundances of Sc and V compared to melts from unfertilized peridotite. We model this scenario using the phase relationship obtained from the BATCH calculations (Fig. 2a, b). Specifically, we assume that HSDP-2 low-SiO_2 lavas are produced by partial melting of a peridotite, whose major element compositions are the same as the primitive mantle from McDonough and Sun (1995), at 1556 °C and 3 GPa with a partial melting degree of 6% (Table 2). Using the phase relations obtained from the BATCH calculations (Table 2) and trace element partition coefficients from literature sources (Table S2), the trace element pattern in the mantle source of the low-SiO_2 lavas is calculated (Fig. 5d). Then the compositions of two mixtures of peridotite and mafic cumulate, 90 + 10% and 95 + 5%, respectively, are calculated. We find that the fertilized source has higher Sc and V abundances than the source of the low-SiO_2 basalt. Then we re-distribute the major elements among the four mineral phases and melt phase using the compositions of these five phases at 1556 °C and 3 GPa. At the same P–T condition, the compositions of each phase are constant, but their relative proportions vary to be consistent with the bulk composition of the sources for the low-SiO_2 and high-CaO lavas. A mixture of 95% peridotite and 5% mafic cumulate at $P = 3$ GPa and $T = 1556$ °C leads to 12% melt, while a mixture of 90% peridotite and 10% mafic cumulate yields 19% melt. For comparison, at this P–T condition, unfertilized peridotite melts to 6% (Table 2). The same exercise has also been done for the mixture of 95% peridotite and 5%

mafic cumulate at 1549 °C and 3 GPa, and leads to 9% partial melting. For comparison, at this P–T, unfertilized peridotite melts to 3% (Table 2). That is, under the same P–T condition, adding a mafic cumulate component to a peridotite leads to a larger degree of partial melting. Trace element patterns in melts are calculated using the phase proportions and partition coefficients in Table 2 and are plotted in Fig. 5a. The important observation is that the highly incompatible element abundances of partial melts vary as a function of both source fertilization and degree of partial melting; however, the abundances of the least incompatible elements, such as Sc and V, remain nearly constant in the partial melts, despite the higher Sc and V abundances in the fertilized peridotite sources (Fig. 5d).

Our calculation shown in Fig. 5 is based on low-SiO_2 and high-CaO parental magma compositions corrected to MgO = 16%, and a peridotite source with the same major element composition as the primitive mantle from McDonough and Sun (1995). Additional model calculations using low-SiO_2 and high-CaO parental magma compositions corrected to MgO = 13% (Fig. S3), and a peridotite source with the same major element composition as the depleted mantle from Workman and Hart (2005) (Fig. S4) reach the same conclusion. We conclude that the Sc and V enrichment in high-CaO lavas is not caused by refertilization of a peridotite source with a clinopyroxene-rich cumulate. This is because a clinopyroxene-rich mantle source leads to high partition coefficients for Sc and V, which are inconsistent with the high Sc and V abundances in the high-CaO lavas (Rhodes et al., 2012).

4.2.3. A role of mafic cumulate: magma-magma mixing

In this scenario, partial melt from pyroxenite, formed from the mafic cumulate, does not mix with partial melt from the peridotite in the mantle, and they migrate to the magma chamber separately. Because of their different solidus temperatures, under the same P–T condition, pyroxenite and peridotite melt to different degrees. For example, at 3 GPa and 1500 °C when a volatile-poor peridotite starts to melt, the mafic lithology melts to a much larger degree, 60–100% (Hirschmann and Stolper, 1996; Walter, 1998; Pertermann and Hirschmann, 2003; Keshav et al., 2004; Pertermann et al., 2004). Specifically, Keshav et al. (2004) experimentally determined the solidus and liquidus temperatures of Salt Lake Crater garnet pyroxenite, a mafic component used in our model calculation (Figs. 5; S5), under 2.0 and 2.5 GPa. Extrapolating their experimental data to 3.0 GPa, the liquidus temperature of Salt Lake Crater garnet pyroxenite is 1500 °C (see Fig. 3 of Keshav et al., 2004). For comparison, under this P–T condition, a peridotite melts to only several percent (see Fig. 4 of Pertermann and Hirschmann, 2003 with data from Walter, 1998; Davis et al., 2011).

We model the trace element pattern in the mixture of high degree melt from pyroxenite and low degree melt from peridotite. The enrichment in highly incompatible elements in high-CaO lavas compared to low-SiO_2 lavas implies a lower degree of partial melting for high-CaO lavas (Rhodes et al., 2012). Consequently, the model to be tested is: The high-CaO lavas represent a mixture of a lower degree partial melt of the low-SiO_2 source and a large degree of melt derived from a mafic cumulate. Following the approach we had in the previous section, we calculate the trace element pattern of unfertilized peridotite (low-SiO_2 source) by assuming that the low-SiO_2 lavas were generated at 1556 °C under 3 GPa with a partial melting degree of 6%. The trace element pattern of high-CaO lavas can be reproduced by mixing 75% of low degree (2%) partial melt of low-SiO_2 source and 25% of a large degree (100%) partial melt of a mafic cumulate (Fig. 5b, c). Specifically, except for Nb and Lu, the modeled melt compositions plot within 1-sigma of the average high-CaO compositions (Figs. 5c, S1b). The differences between the modeled melt compositions and the average high-CaO compositions are less than 15% for all elements, except for Nb (30%) and Lu (20%) (Fig. S1b).

Here, we assumed that when low-SiO_2 source melts to 2%, the mafic cumulate melts completely. Under this scenario, the most incompatible element enrichment in high-CaO lavas compared to low-SiO_2 lavas represents a smaller degree of partial melting (Rhodes et al., 2012), and the Sc-V enrichment represents a role of clinopyroxene-rich mafic cumulate. Compared to low-SiO_2 lavas, high-CaO lavas do not have a positive Sr anomaly. This is because the Sr-peak in the mafic cumulate (e.g., Fig. 5d) caused by plagioclase accumulation is masked by the high abundances of highly to moderately incompatible elements in the low degree partial melt (Fig. 5c). This is different from the model presented in Frey et al. (this issue), in which the positive Sr anomaly of mafic cumulate is still preserved in the mixture of partial melt of peridotite (Kilauea lava in their case) and melt of mafic cumulate. This later effect is caused by the low abundances of highly to moderately incompatible elements of partial melt of peridotite used in Frey et al. (this issue); consequently, the positive Sr anomaly of the mafic cumulate is not completely diluted in the mixture.

In order to test the sensitivity of our model, additional model calculations are presented. Such calculations include using low-SiO_2 and high-CaO parental magma compositions corrected to MgO = 13% (Fig. S3), using a peridotite source with the same major element composition as the depleted mantle from Workman and Hart (2005) (Fig. S4), and using Salt Lake Crater garnet pyroxenite (Bizimis et al., 2005; Sen et al., 2011) (Fig. S5). In all cases, the modeled compositions of mixtures are within 1-sigma of the average high-CaO lavas. Specifically, if the Salt Lake Crater garnet pyroxenite is used, the element pattern of high-CaO lavas can be reproduced by mixing 60% of a low degree (1.5%) partial melt of low-SiO_2 source and 40% of a high degree (100%) partial melt of mafic cumulate (Fig. S5).

In our calculations discussed above, the clinopyroxene-rich mafic cumulate is assumed to melt to 100%. Additional calculations show that the high-CaO lava trace element pattern can also be reproduced if the clinopyroxene-rich mafic cumulate does not melt completely (Figs. S6, S7). Specifically, the trace element pattern of high-CaO lavas can be reproduced by mixing 65–70% low degree (2%) partial melt of the low-SiO_2 mantle source and 30–35% high degree (80%) partial melt of a mafic cumulate (Figs. S6, S7).

4.2.4. Origin of the mafic cumulate sampled by high-CaO lavas

There are three types of tectonic setting under which a clinopyroxene-rich mafic cumulate can form: a mafic cumulate delaminated during the formation of continental crust under arcs (e.g., Lee et al., 2012; Jagoutz and Schmidt, 2013), under the lower continental crust (e.g., McKenzie and O'Nions, 1983), or under the lower oceanic crust (e.g., Hart et al., 1999). High pressure cumulates, such as garnet pyroxenites from Salt Lake Crater, Hawaii (Frey, 1980; Bizimis et al., 2005; Sen et al., 2011) are also potential candidates. All these mafic cumulates are basically clinopyroxene-rich cumulates with similar trace element patterns (Fig. 5d; also see Frey et al., this issue, for a detailed discussion, and compare Fig. 9 of Hart et al., 1999; Fig. 2 of Jagoutz and Schmidt, 2013 and Fig. 9 of Mansur et al., 2014). Although in our model calculations, we used the mafic cumulate formed under arcs during continent formation (Jagoutz and Schmidt, 2013) (Fig. 5) and formed as high pressure cumulates (Salt Lake Crater garnet pyroxenite; Bizimis et al., 2005; Sen et al., 2011) (Fig. S5), we do not exclude the possibility that the mafic component sampled by high-CaO lavas can also be lower continental crust. A critical requirement is that the mafic cumulate must have Sc and V abundances high enough so that its signature can be observed in the mixture, which implies a high proportion of clinopyroxene in the mafic cumulate. The lower oceanic crust (gabbroic crust) studied by Hart et al. (1999) has high Sc abundance, but not high V abundance (Fig. 5d); consequently, sampling this type of lower oceanic crust cannot explain the high V abundance in HSDP-2 high-CaO lavas.

Willbold and Stracke (2006) used highly to moderately incompatible element ratios to identify the roles of recycled sediments and lithosphere in the mantle sources of oceanic basalts. In our study, arc mafic cumulate has Ba/Th higher than the primitive mantle value, and Salt Lake City cumulate has Ba/Th lower than the primitive mantle value (Fig. 5d). However, both types of cumulates are able to reproduce the high-CaO lava composition with Ba/Th higher than the primitive mantle value (Figs. 5b, c vs. S5). This is because the low degree partial melt of peridotite in our model has high abundances of highly to moderately incompatible elements; consequently, the distinctive characteristics of highly incompatible elements in these cumulates, such as Ba/Th and positive Sr anomaly, are masked in the mixture.

The clinopyroxene-rich cumulates may be recycled back or delaminated into the convecting mantle, entrained into the upwelling Hawaiian plume, and finally sampled during partial melting that contributed to Hawaiian volcanoes. It is also possible that the clinopyroxene-rich cumulates were sampled by melt-rock reaction during magma ascent, similar to the model proposed by Eggins (1992) and Wagner and Grove (1998). In this case, a clinopyroxene-rich cumulate, such as the lower oceanic gabbroic crust or high-pressure cumulate in a magma chamber of a previous Hawaiian volcano, is melted and sampled by ascending magma from the Hawaiian plume. The difference between melting of a clinopyroxene-rich cumulate in the mantle source and assimilation of a clinopyroxene-rich cumulate during ascent of high-CaO magmas may be discriminated by future work using radiogenic isotopes.

4.3. Fe/Mn of HSDP-2 high-CaO lavas

The Fe/Mn of Hawaiian tholeiites is systematically higher than that of MORB or Icelandic tholeiites (Humayun et al., 2004; Qin and Humayun, 2008). Is the Hawaiian plume richer in Fe, as might be expected from chemical interactions at the core-mantle boundary (Humayun et al., 2004), or is Mn retained in the mantle sources of intraplate lavas (Sobolev et al., 2005, 2007)? One prediction of models that invoke pyroxenite to retain Mn in the mantle source is that Fe/Mn should vary as the fraction of pyroxenite in the source is inferred to vary from ~50% to over 90% (Sobolev et al., 2007). Huang et al. (2007) showed that the high Fe/Mn observed in Hawaiian lavas are a general characteristic of all major Hawaiian volcanoes, including Makapuu-stage Koolau lavas that are thought to have the highest pyroxenite contributions. These workers also found that the Fe/Mn was not significantly changed by the addition of dacitic melts from pyroxenite sources (Huang and Frey, 2005), which are characteristically low in both Fe and Mn. Such dacitic melts can influence the distinct radiogenic isotopes and trace element characteristics of Koolau vs. Loihi (Huang and Frey, 2005). How is the Fe/Mn affected when the source composition is sufficiently extreme to influence the least compatible element abundances (e.g., Sc)?

HSDP-2 high-CaO glasses have Fe/Mn similar to other Hawaiian shield lavas and plot at the low-MgO end of the olivine-control trend defined by Kilauea lavas (Fig. 3). We showed that high-CaO lavas may have sampled a mafic component that formed as clinopyroxene-rich cumulates. Clinopyroxene has a low Fe/Mn (e.g., Pertermann and Hirschmann, 2003; Humayun et al., 2004; Davis et al., 2013), so clinopyroxene assimilation or melts from a clinopyroxene-rich source might be expected to lower the Fe/Mn in the magma. For example, the delaminated mafic cumulate under arcs has FeO of 12.8% and Fe/Mn of 58 (Jagoutz and Schmidt, 2013). Under the magma-magma mixing scenario (case A of Fig. 6; see discussion in Section 4.2.3), high-CaO lavas represent a mixture of 60–75% low degree partial melt of low-SiO_2 mantle source and 25–40% high degree (80–100%) partial melt of a mafic cumulate. If the low degree partial melt of the low-SiO_2 lavas mantle source has the typical Hawaiian lava composition with FeO of 12% and Fe/Mn of 66, and the high degree (>80%) partial melts of pyroxenite have essentially the same Fe/Mn as their source (see Fig. 7 of Huang et al., 2007 with data from Pertermann and Hirschmann, 2003), the magma-magma mixing models discussed in Section 4.2.3 would yield a Fe/Mn of 62.4–63.7 in the mixture. This small Fe/Mn effect is consistent with high-CaO glasses plotting at the low-MgO end of the Kilauea trend in a MgO-Fe/Mn diagram (Fig. 3). That is, the high Fe/Mn ratio (>63) is a feature of the dominantly peridotite sources of all Hawaiian magmas.

5. SUMMARY

(1) BATCH (Longhi, 2002) calculations show that CaO contents in melts saturated with all four mineral phases in garnet peridotite are functions of both degrees of partial melting and source heterogeneity. Consequently, melt CaO content may not be able to distinguish between partial melting of garnet peridotite and garnet pyroxenite/eclogite, consistent with Herzberg et al. (2014).

(2) Compared to HSDP-2 low-SiO_2 lavas, high-CaO lavas have higher abundances of highly incompatible and least incompatible elements, and similar moderately incompatible element abundances. When normalized to HSDP-2 low-SiO_2 lavas, high-CaO lavas form a U-shaped trace element pattern. It is inferred that high-CaO lavas are a mixture of a low degree (~2%) partial melt of the low-SiO_2 peridotite source and a high degree melt of a mafic component rich in cumulate clinopyroxene. The clinopyroxene-rich cumulates may have formed beneath arcs during continent formation, in the lower continental crust, or as high pressure cumulates.

(3) Hawaiian lavas, including Makapuu-stage Koolau lavas (high-SiO_2 and low-CaO end) and Mauna Kea HSDP-2 high-CaO glasses (low-SiO_2 and high-CaO end), have similar Fe/Mn, which is significantly higher than that of MORB and Icelandic lavas. This study confirms that high Fe/Mn is a general property of the sources of Hawaiian lavas, independent of the composition or extent of pyroxenite in the source.

ACKNOWLEDGEMENTS

We thank D. DePaolo, E. Stolper, and D. Thomas for their leadership of the HSDP, M. O. Garcia, C. Seaman and the logging crew for their on-site efforts, M. Baker and E. M. Stolper for loaning the high-CaO glass mounts, and C. Herzberg, F. Frey and J. M. Rhodes for stimulating this project. Specifically, we thank M. Baker for the BATCH calculations. We thank M. Baker, F. Frey, C. Herzberg, J. M. Rhodes and E. Stolper for numerous discussions and critical but constructive comments. Comments from M. Bizimis and an anonymous reviewer, as well as Guest Editor M. O. Garcia, significantly improved this manuscript. SH acknowledges support from NSF awards EAR-1524387 and EAR-1144727.

APPENDIX A. SUPPLEMENTARY DATA

Supplementary data associated with this article can be found, in the online version, at http://dx.doi.org/10.1016/j.gca.2016.03.039.

REFERENCES

Abouchami W. (2007) Coupled major element-lead isotope variability in Hawaiian lavas. A3 2007 Goldschmidt Conference Abstracts.

Adam J. and Green T. (2006) Trace element partitioning between mica- and amphibole-bearing garnet lherzolite and hydrous basanitic melt: 1. Experimental results and the investigation of controls on partitioning behavior. *Contrib. Mineral Petrol.* **152**, 1–17.

Balta J. B., Asimow P. D. and Mosenfelder J. L. (2011) Hydrous, Low-carbon melting of garnet peridotite. *J. Petrol.* **52**, 2079–2105. http://dx.doi.org/10.1093/petrology/egr040.

Bizimis M., Sen G., Salters V. J. M. and Keshav S. (2005) Hf-Nd-Sr isotope systematics of garnet pyroxenites from Salt Lake Crater, Oahu, Hawaii: evidence for a depleted component in Hawaiian volcanism. *Geochim. Cosmochim. Acta* **69**, 2629–2646. http://dx.doi.org/10.1016/j.gca.2005.01.005.

Blichert-Toft J. and Albarède F. (2009) Mixing of isotopic heterogeneities in the Mauna Kea plume conduit. *Earth Planet Sci. Lett.* **282**, 190–200. http://dx.doi.org/10.1016/j.epsl.2009.03.015.

Blichert-Toft J., Weis D., Maerschalk C., Agrainer A. and Albarède F. (2003) Hawaiian hotspot dynamics sas inferred from the Hf and Pb isotope evolution of Mauna Kea volcano. *Geochem. Geophys. Geosyst.* **4**, 8704. http://dx.doi.org/10.1029/2002GC000340.

Brandon A. D., Norman M. D., Walker R. J. and Morgan J. W. (1999) ^{186}Os-^{187}Os systematics of Hawaiian picrites. *Earth Planet Sci. Lett.* **172**, 25–42.

Bryce J., DePaolo D. J. and Lassiter J. C. (2005) Geochemical structure of the Hawaiian plume: Sr, Nd and Os isotopes in the 2.8 km HSDP-2 section of Mauna Kea volcano. *Geochem. Geophys. Geosyst.* **6**, Q09G18. http://dx.doi.org/10.1029/2004GC000809.

Chauvel C. and Hémond C. (2000) Melting of a complete section of recycled oceanic crust: trace element and Pb isotopic evidence from Iceland. *Geochem. Geophys. Geosyst.* **1**. http://dx.doi.org/10.1029/1999GC000002.

Dasgupta R., Jackson M. G. and Lee C.-T. (2010) Major element chemistry of ocean island basalts – Conditions of mantle melting and heterogeneity of mantle source. *Earth Planet. Sci. Lett.* **289**, 377–392. http://dx.doi.org/10.1016/j.epsl.2009.11.027.

Davis F. A., Hirschmann M. M. and Humayun M. (2011) The composition of the incipient partial melt of garnet peridotite at 3 GPa and the origin of OIB. *Earth Planet. Sci. Lett.* **308**, 380–390. http://dx.doi.org/10.1016/j.epsl.2011.06.008.

Davis F. A., Humayun M., Hirschmann M. M. and Cooper R. S. (2013) Experimentally determined mineral/melt partitioning of first-row transition elements (FRTE) during partial melting of peridotite at 3 GPa. *Geochim. Cosmochim. Acta* **104**, 232–260. http://dx.doi.org/10.1016/j.gca.2012.11.009.

Eggins S. M. (1992) Petrogenesis of Hawaiian tholeiites: 1. Phase equilibria constraints. *Contrib. Mineral. Petrol.* **110**, 387–397.

Eisele J., Abouchami W., Galer S. J. G. and Hofmann A. W. (2003) The 320 kyr Pb isotope evolution of Mauna Kea lavas recorded in the HSDP-2 drill core. *Geochem. Geophys. Geosyst.* **4**(5), 8710. http://dx.doi.org/10.1029/2002GC000339.

Ford C. E., Russell J. A. and Fisk M. R. (1983) Olivine liquid equilibria: temperature, pressure and composition dependence on the crystal/liquid cation partition coefficients for Mg, Fe^{2+}, Ca and Mn. *J. Petrol.* **24**, 256–265.

Frey F. A. and Clague D. A. (1983) Geochemistry of diverse basalt types from Loihi Seamount, Hawaii; petrogenetic implications. *Earth Planet. Sci. Lett.* **66**, 337–355.

Frey F. A., Garcia M. O. and Roden M. F. (1994) Geochemical characteristics of Koolau Volcano: implications of intershield geochemical differences among Hawaiian volcanoes. *Geochim. Cosmochim. Acta.* **58**, 1441–1462.

Frey F.A., Huang S. and Xu G. Plagioclase and clinopyroxene cumulate in the source of Hawaiian shield basalt: evidence based on abundance ratios of incompatible elements. *Geochim. Cosmochim. Acta* (this issue).

Frey F. A. (1980) The origin of pyroxenites and garnet pyroxenites from Salt Lake Crater, Oahu, Hawaii: trace element evidence. *Am. J. Sci.* **208A**, 427–449.

Gale A., Dalton C. A., Langmuir C. H., Su Y. and Schilling J.-G. (2013) The mean composition of ocean ridge basalts. *Geochem. Geophys. Geosyst* **14**, 489–518. http://dx.doi.org/10.1029/2012GC004334.

Garcia M. O., Jorgenson B., Mahoney J. J., Ito E. and Irving A. J. (1993) An evaluation of temporal geochemical evolution of Loihi Seamount lavas: results from Alvin submersible dives. *J. Geophys. Res.* **98**, 357–380.

Garcia M. O., Foss D. J. P., West H. B. and Mahoney J. J. (1995) Geochemical and isotopic evolution of Loihi Volcano, Hawaii. *J. Petrol.* **36**, 1647–1671.

Garcia M. O., Rubin K. H., Norman M. D., Rhodes J. M., Graham D. W., Muenow D. and Spencer K. (1998) Petrology and geochronology of basalt breccia from the 1996 earthquake swarm of Loihi Seamount, Hawaii: magmatic history of its 1996 eruption. *Bull. Volcanol.* **59**, 577–592.

Garcia M. O., Haskins E. H., Stolper E. M. and Baker M. (2007) Stratigraphy of the Hawai'i Scientific Drilling Project core (HSDP2): Anatomy of a Hawaiian shield volcano. *Geochem. Geophys. Geosyst.* **8**, Q02G20. http://dx.doi.org/10.1029/2006GC001379.

Ghiorso M. S., Hirschmann M. M., Reiners P. W. and Kress, III, V. C. (2002) The pMELTS: a revision of MELTS for improved calculation of phase relations and major element partitioning related to partial melting of the mantle to 3 GPa. *Geochem. Geophys. Geosyst.* **3**, 1030.

Hart S. R. and Dunn T. (1993) Experimental cpx/melt partitioning of 24 trace elements. *Contrib. Mineral Petrol.* **113**, 1–8.

Hart S. R., Blusztajn J., Dick H. J. B., Meyer P. S. and Muehlenbachs K. (1999) The fingerprint of seawater circulation in a 500-meter section of ocean crust gabbros. *Geochim. Cosmochim. Acta* **63**, 4059–4080.

Hauri E. H. (1996) Major-element variability in the Hawaiian mantle plume. *Nature* **382**, 415–419.

Herzberg C., Cabral R. A., Jackson M. G., Vidito C., Day J. M. D. and Hauri E. H. (2014) Phantom Archean crust in Mangaia hotspot lavas and the meaning of heterogeneous mantle. *Earth Planet. Sci. Lett.* **396**, 97–106. http://dx.doi.org/10.1016/j.epsl.2014.03.065.

Herzberg C. (2006) Petrology and thermal structure of the Hawaiian plume from Mauna Kea volcano. *Nature* **444**, 605–609. http://dx.doi.org/10.1038/nature05254.

Herzberg C. (2011) Identification of source lithology in the Hawaiian and Canary Islands: implications for origins. *J. Petrol.* **52**, 113–146. http://dx.doi.org/10.1093/petrology/egq075.

Hill E., Blundy J. D. and Wood B. J. (2011) Clinopyroxene-melt trace element partitioning and the development of a predictive model for HFSE and Sc. *Contrib. Mineral. Petrol.* **161**, 423–438. http://dx.doi.org/10.1007/s00410-010-0540-0.

Hirschmann M. M. and Stolper E. M. (1996) A possible role for garnet pyroxenite in the origin of the "garnet signature" in MORB. *Contrib. Mineral. Petrol.* **124**, 185–208.

Hofmann A. W. and White W. M. (1982) Mantle plumes from ancient oceanic crust. *Earth Planet. Sci. Lett.* **57**, 421–436.

Huang S. and Frey F. A. (2003) Trace element abundances of Mauna Kea basalt from Phase 2 of the Hawaiian Scientific Drilling Project: petrogenetic implications of correlations with major element content and isotopic ratios. *Geochem. Geophys. Geosyst.* **4**(6), 8711, 1029/2002GC000322.

Huang S. and Frey F. A. (2005) Recycled oceanic crust in the Hawaiian Plume: evidence from temporal geochemical variations within the Koolau Shield. *Contrib. Mineral. Petrol.* **149**, 556–575. http://dx.doi.org/10.1007/s00410-005-0664-9.

Huang S., Frey F. A., Blichert-Toft J., Fodor R. V., Bauer G. R. and Xu G. (2005) Enriched components in the Hawaiian plume: evidence from Kahoolawe Volcano, Hawaii. *Geochem. Geophys. Geosyst.* **6**, Q01L06. http://dx.doi.org/10.1029/2004GC000756.

Huang S., Humayun M. and Frey F. A. (2007) Iron/manganese ratio and manganese content in shield lavas from Ko'olau Volcano, Hawai'i. *Geochim. Cosmochim. Acta* **71**, 4557–4569. http://dx.doi.org/10.1016/j.gca.2007.07.013.

Humayun M., Qin L. and Norman M. D. (2004) Geochemical evidence for excess iron in the mantle beneath Hawai'i. *Science* **306**, 91–94.

Humayun M., Simon S. B. and Grossman L. (2007) Tungsten and hafnium distribution in calcium-aluminum inclusions (CAIs) from Allende and Efremovka. *Geochim. Cosmochim. Acta* **71**, 4609–4627.

Jackson M. G. and Dasgupta R. (2008) Compositions of HIMU, EM1, and EM2 from global trends between radiogenic isotopes and major elements in ocean island basalts. *Earth Planet. Sci. Lett.* **276**, 175–186. http://dx.doi.org/10.1016/j.epsl.2008.09.023.

Jackson M. G., Weis D. and Huang S. (2012) Major element variations in Hawaiian shield lavas: source features and perspectives from global ocean island basalt (OIB) systematics. *Geochem. Geophys. Geosyst.* **13**, Q09009. http://dx.doi.org/10.1029/2012GC004268.

Jagoutz O. and Schmidt M. W. (2013) The composition of the foundered complement to the continental crust and a re-evaluation of fluxes in arcs. *Earth Planet. Sci. Lett.* **371–372**, 177–190. http://dx.doi.org/10.1016/j.epsl.2013.03.051.

Jochum K. P. et al. (2006) MPI-DING reference glasses for in situ microanalysis: new reference values for element concentrations and isotope ratios. *Geochem. Geophys. Geosyst.* **7**, Q02008. http://dx.doi.org/10.1029/2005GC001060.

Jourdan F. W., Sharp W. D. and Renne P. R. (2012) $^{40}Ar/^{39}Ar$ ages for deep (~3.3 km) samples from the Hawaii Scientific Drilling Project, Mauna Kea volcano, Hawaii. *Geochem. Geophys. Geosyst.* **13**, Q05004. http://dx.doi.org/10.1029/2011GC004017.

Keshav S., Gudfinnsson G. H., Sen G. and Fei Y. (2004) High-pressure melting experiments on garnet clinopyroxenite and the alkalic to tholeiitic transition in ocean-island basalts. *Earth Planet. Sci. Lett.* **223**, 365–379. http://dx.doi.org/10.1016/j.epsl.2004.04.029.

Kogiso T. and Hirschmann M. M. (2006) Partial melting experiments of bimineralic eclogite and the role of recycled mafic oceanic crust in the genesis of ocean island basalts. *Earth Planet. Sci. Lett.* **249**, 188–199. http://dx.doi.org/10.1016/j.epsl.2006.07.016.

Kurz M. D., Curtice J., Lott, III, D. E. and Solow A. (2004) Rapid helium isotopic variability in Mauna Kea shield lavas from the Hawaiian Scientific Drilling Project. *Geochem. Geophys. Geosyst.* **5**, Q04G14. http://dx.doi.org/10.1029/2002GC000439.

Lassiter J. C. and Hauri E. H. (1998) Osmium-isotope variations in Hawaiian lavas: evidence for recycled oceanic lithosphere in the Hawaiian plume. *Earth Planet. Sci. Lett.* **164**, 483–496.

Lee C.-T. A., Leeman W. P., Canil D. and Li Z.-X. A. (2005) Similar V/Sc systematics in MORB and Arc basalts: implications for the oxygen fugacities of their mantle source regions. *J.*

Petrol. **46**, 2313–2336. http://dx.doi.org/10.1093/petrology/egi056.

Lee C.-T., Luffi P., Chin E. J., Bouchet R., Dasgupta R., Morton D. M., Le Roux V., Yin Q.-Z. and Jin D. (2012) Copper systematics in arc magmas and implications for crust-mantle differentiation. *Science* **336**, 64–68. http://dx.doi.org/10.1126/science.1217313.

Longhi J. (2002) Some phase equilibrium systematics of lherzolite melting: I. *Geochem. Geophys. Geosyst.* **3**(3). http://dx.doi.org/10.1029/2001GC000204.

Mansur A. T., Manya S., Timpa S. and Rudnick R. L. (2014) Granulite-facies xenoliths in rift basalts of northern Tanzania: age, composition and origin of Archean lower crust. *J. Petrol.* **55**, 1243–1286. http://dx.doi.org/10.1093/petrology/egu024.

McDonough W. F. and Sun S.-S. (1995) The composition of the Earth. *Chem. Geol.* **120**, 223–253.

McKenzie D. and O'Nions R. K. (1983) Mantle reservoirs and ocean island basalts. *Nature* **301**, 229–231.

Montelli R., Nolet G., Dahlen F. A., Masters G., Engdahl E. R. and Hung S.-H. (2004) Finite-frequency tomography reveals a variety of plumes in the mantle. *Science* **303**, 338–343. http://dx.doi.org/10.1126/science.1092485.

Nobre Silva I. G., Weis D. and Scoates J. S. (2013) Isotopic systematics of the early Mauna Kea shield phase and insight into the deep mantle beneath the Pacific Ocean. *Geochem. Geophys. Geosyst.* **14**. http://dx.doi.org/10.1002/ggge.20047.

Norman M. D. and Garcia M. O. (1999) Primitive magmas and source characteristics of the Hawaiian Plume; petrology and geochemistry of shield picrites. *Earth Planet Sci. Lett.* **168**, 27–44.

Pearce N. J. G., Perkins W. T., Westgate J. A., Gorton M. P., Jackson S. E., Neal C. R. and Chenery S. P. (1997) A compilation of new and published major and trace element data for NIST SRM 610 and NIST SRM 612 glass reference materials. *Geostand. Newsl.* **21**, 115–144.

Pertermann M. and Hirschmann M. M. (2003) Partial melting experiments on a MORB-like pyroxenite between 2 and 3 GPa: constraints on the presence of pyroxenite in basalt source regions from solidus location and melting rate. *J. Geophys. Res.* **108**(B2), 2125. http://dx.doi.org/10.1029/2000JB000118.

Pertermann M., Hirschmann M. M., Hametner K., Gunther D. and Schmidt M. W. (2004) Experimental determination of trace element partitioning between garnet and silica-rich liquid during anhydrous partial melting of MORB-like eclogite. *Geochem. Geophys. Geosyst.* **5**, Q05A01. http://dx.doi.org/10.1029/2003GC000638.

Pietruszka A. J., Norman M. D., Garcia M. O., Marske J. P. and Burns D. H. (2013) Chemical heterogeneity in the Hawaiian mantle plume from the alteration and dehydration of recycled oceanic crust. *Earth Planet. Sci. Lett.* **361**, 298–309. http://dx.doi.org/10.1016/j.epsl.2012.10.030.

Putirka K., Ryerson F. J., Perfit M. and Ridley W. I. (2011) Mineralogy and composition of the oceanic mantle. *J. Petrol.* **52**, 279–313.

Qin L. and Humayun M. (2008) The Fe/Mn ratio in MORB and OIB determined by ICP-MS. *Geochim. Cosmochim. Acta* **72**, 1660–1677. http://dx.doi.org/10.1016/j.gca.2008.01.012.

Rhodes J. M. and Vollinger M. J. (2004) Composition of basaltic lavas sampled by phase-2 of the Hawai'i Scientific Drilling Project: geochemical stratigraphy and magma types. *Geochem. Geophys. Geosyst.* **5**, Q03G13. http://dx.doi.org/10.1029/2002GC000434.

Rhodes J. M., Huang S., Frey F. A., Pringle M. and Xu G. (2012) Compositional diversity of Mauna Kea shield lavas recovered by the Hawaii Scientific Drilling Project: inferences on source lithology, magma supply, and the role of multiple volcanoes. *Geochem. Geophys. Geosyst.* **13**(3), Q03014. http://dx.doi.org/10.1029/2011GC003812.

Rhodes J.M. (2016) The aluminum conundrum in Hawaiian shield-building lavas: an argument for a deep, garnet-bearing, mantle source. *Geochim. Cosmochim. Acta* **185,** 216–231.

Rudnick R. L. and Gao S. (2003) Composition of the Continental Crust. In *The Crust* (ed. R. L. Rudnick). Elsevier-Pergamon, Oxford, pp. 1–64.

Salters V. J. M., Blichert-Toft J., Fekiacova Z., Sachi-Kocher A. and Bizimis M. (2006) Isotope and trace element evidence for depleted lithosphere in the source of enriched Ko'olau basalts. *Contrib. Mineral. Petrol.* **151**(3), 297–312.

Sen I. S., Bizimis M., Sen G. and Huang S. (2011) A radiogenic Os component in the oceanic lithosphere? Constraints from Hawaiian pyroxenite xenoliths. *Geochim. Cosmochim. Acta* **75**, 4899–4916. http://dx.doi.org/10.1016/j.gca.2011.06.008.

Sobolev A. V., Hofmann A. W., Sobolev S. V. and Nikogosian I. K. (2005) An olivine free mantle source of Hawaiian shield basalts. *Nature* **434**, 590–597. http://dx.doi.org/10.1038/nature03411.

Sobolev A. V., Hofmann A. W., Kuzmin D. V., Yaxley G. M., Arndt N. T., Chung S.-L., Garcia M. O., Gurenko A. A., Danyushevsky L. V., Elliott T., Frey F. A., Kamenetsky V. S., Kerr A. C., Krivolutskaya N. A., Matvienkov V. V., Nikogosian I. K., Rocholl A., Suschevskaya N. M. and Teklay M. (2007) The amount of recycled crust in sources of mantle-derived melts. *Science* **316**, 412–417. http://dx.doi.org/10.1126/science.1138113.

Stolper E. M., DePaolo D. J. and Thomas D. M. (1996) Introduction to special section; Hawaii Scientific Drilling Project. *J. Geophys. Res.* **101**(11593–11598), 1996.

Stolper E., Sherman S., Garcia M., Baker M. and Seaman C. (2004) Glass in the submarine section of the HSDP2 drill core, Hilo, Hawai'i. *Geochem. Geophys. Geosyst.* **5**, Q07G15. http://dx.doi.org/10.1029/2003GC000553.

Stolper E. M., DePaolo D. J. and Thomas D. M. (2009) Deep drilling into a mantle plume volcano: the Hawaii Scientific Drilling Project. *Sci. Drill.* **7**, 4–14.

Taylor S. R. and McLennan S. M. (2009) *Planetary Crusts: Their Composition, Origin, and Evolution*. Cambridge University Press, Cambridge, 378pp.

Wagner T. P. and Grove T. L. (1998) Melt/harzburgite reaction in the petrogenesis of tholeiitic magma from Kilauea Volcano. *Hawai'i. Contrib. Mineral. Petrol.* **131**(1), 1–12.

Walter M. J. (1998) Melting of garnet peridotite and the origin of komatiite and depleted lithosphere. *J. Petrol.* **39**(1), 29–60.

Willbold M. and Stracke A. (2006) Trace element composition of mantle end-members: implications for recycling of oceanic and upper and lower continental crust. *Geochem. Geophys. Geosyst.* **7**, Q04004. http://dx.doi.org/10.1029/2005GC001005.

Wilson J. T. (1963) A possible origin of the Hawaiian Islands. *Can. J. Phys.* **41**, 863–870.

Workman R. K. and Hart S. R. (2005) Major and trace element composition of the depleted MORB mantle (DM). *Earth Planet Sci. Lett.* **231**, 53–72. http://dx.doi.org/10.1016/j.epsl.2004.12.005.

Associate editor: Michael Garcia